Supporting Information

Iodide Oxidation Reaction Catalyzed by Ruthenium-Tin Surface Alloy Oxide for Efficient Production of Hydrogen and Iodine Simultaneously

Dessalew Berihun Adam [1], Meng-Che Tsai [2,4,] *, Yohannes Ayele Awoke [1], Wei-Hsiang Huang[2], Yaw-Wen Yang[3,] Chih-Wen Pao[3], Wei-Nien Su[2,4,] *, and Bing Joe Hwang [1,2,3,4] *

[1]NanoElectrochemistry Laboratory, Department of Chemical Engineering, National Taiwan University of Science and Technology, Taipei 10607, Taiwan

[2]NanoElectrochemistry Laboratory, Graduate Institute of Applied Science and Technology, National Taiwan University of Science and Technology, Taipei 10607, Taiwan

[3]National Synchrotron Radiation Research Center, Hsin-Chu 30076, Taiwan

[4]Sustainable Energy Development Center, National Taiwan University of Science and Technology, Taipei 106, Taiwan.

*Corresponding authors:

bjh@mail.ntust.edu.tw (Bing Joe Hwang)

wsu@mail.ntust.edu.tw (Wei-Nien Su)

mctsai@mail.ntsut.edu.tw (Meng-Che Tsai)

Number of pages:15

Number of figures:13

Number of Tables:8

Table of contents

Figure S1. Raman spectra for RuO_2 and SnO_2.....S4

Figure S2. Energy-dispersive X-ray spectroscopy (EDX) profile of as-prepared RuSn SAO.....S4

Figure S3. Wide range XPS spectra for SnO_2, RuO_2 and RuSn SAO samples.....S5

Table S1: The relative sensitivity factor of the element Ru, Sn and O.....S6

Table S2. XPS fitting results and calculated values in RuSn SAO sample.....S6

Table S3: Estimated elemental composition of RuSn SAO sample.....S6

Figure S4. EXAFS fitting spectra.....S7

Table S4. FT-EXAFS analysis results for the RuO_2 and RuSn SAO.....S8

Figure S5. CV for commercial Pt/C in IOR at different scan rates.....S8

Figure S6. CV for SnO_2 in IOR at different scan rates.....S9

Figure S7. CV for IOR at the different scan rates for the RuSn SAO electrocatalyst and current densities plotted against the scan rate.....S9

Figure S8. Peak-to-peak separation potentials at scan rate of 50 mV/s.....S10

Table S5. Summary of electrochemical surface area, roughness factor, double layer capacitance and mass activity.....S11

Figure S9. LSV curves for RuSn SAO in 0.1 M $HClO_4$ with different NaI concentrations; LSVcurves of RuSn SAO before and after stability in 0.1 M $HClO_4$ with NaI solution, and rate of hydrogen production per time of electrolysis.....S11

Figure S10. Chronopotentiometric stability for OER at applied current density of 10 $mAcm^{-2}$....S12

Figure S11. CV curves for as-prepared samples from non-Faradaic regions.....S12

Figure S12. Hydrogen detection by gas chromatography (GC).....S13

Table S6. Electrochemical performance of Ru-based oxide electrocatalysts for IOR-based electrolysis developed in this work and for OER-based electrolysis reported in literatures.....S13

Table S7. Summary of electrochemical parameters of catalysts in IOR obtained from CV and LSV curves.....S14

Table S8. Metal analysis by ICP-MS from RuSn SAO sample.....S14

Figure S13. ICP-MS calibration curves for (a) Ru and (b) Sn elements.....S14

References.....S15

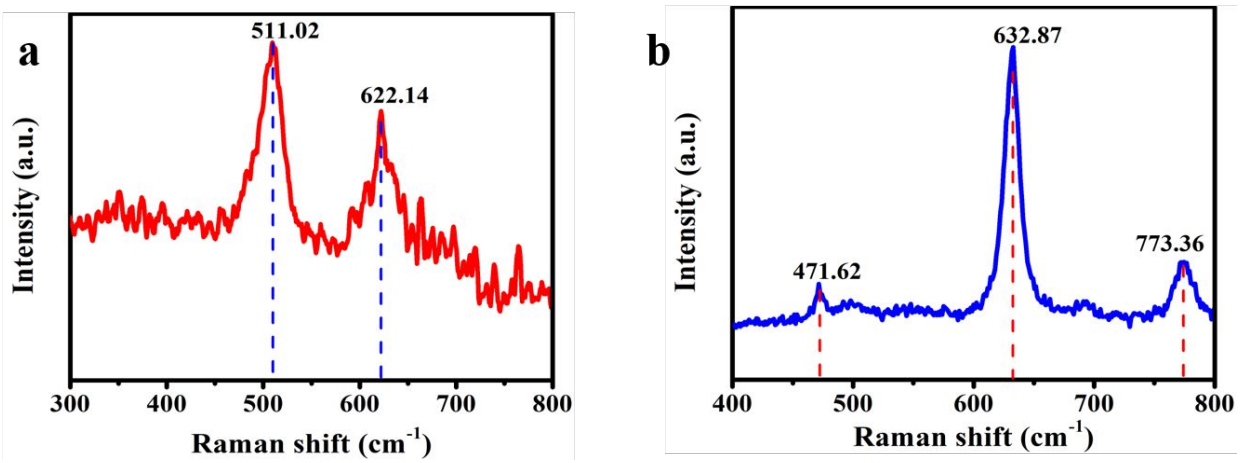

Figure S1. Raman spectra for (a) RuO_2 (b) SnO_2

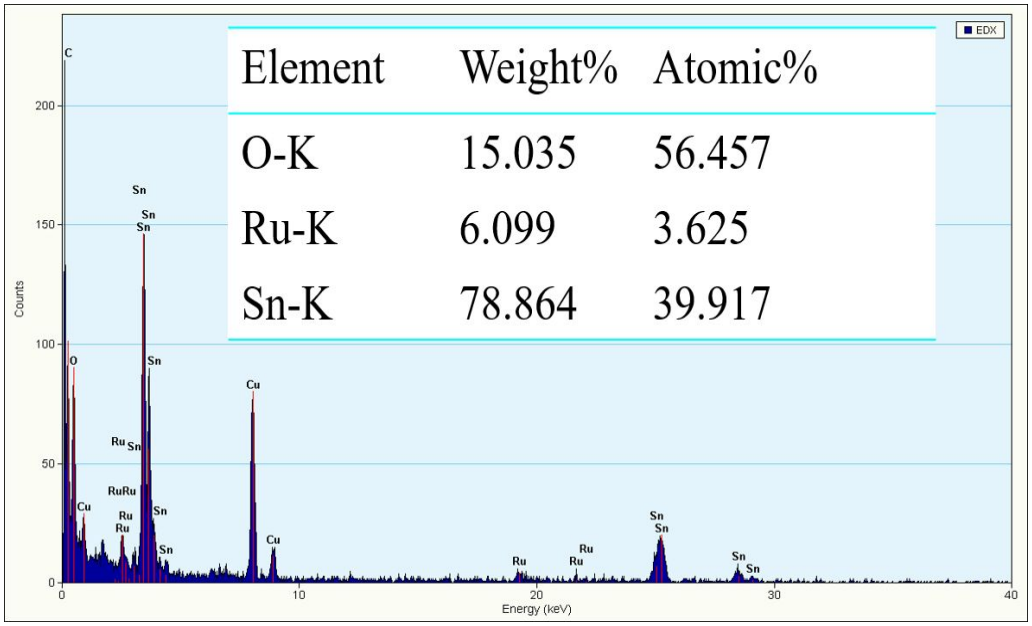

Element	Weight%	Atomic%
O-K	15.035	56.457
Ru-K	6.099	3.625
Sn-K	78.864	39.917

Figure S2. Energy-dispersive X-ray spectroscopy (EDX) profile of as-prepared RuSn SAO.

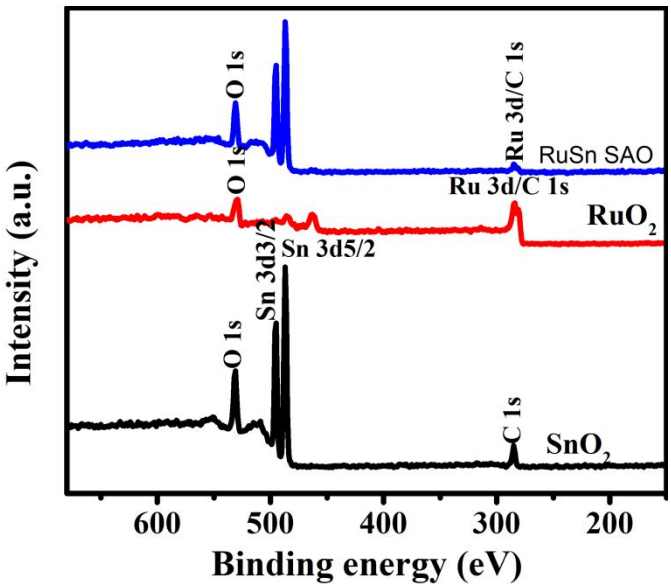

Figure S3. Wide range XPS spectra for SnO_2, RuO_2 and RuSn SAO samples.

Atomic Ratio Calculation from XPS in RuSn SAO sample

The atomic ratios of Ru, Sn and O in the sample of RuSn SAO have been calculated using the following equation:

$$\frac{Ix/Sx}{\sum Ix/Sx} \quad \text{(S1)}$$

Where, C_X is atomic ratio, I_X is area from the fitted peaks of the atom and S_X is relative sensitivity factor (RSF) and it is tubular value. The relative sensitivity factor of Ru, Sn and O are listed in Table1-2 below:

Table S1: The relative sensitivity factor of the element Ru, Sn and O, normalized C 1s = 1

Element	line	RSF	Element	line	RSF
Ru	3d5/2	7.39	Ru	3d3/2	5.10
	3p3/2	6.78		3p1/2	3.83
Sn	3d5/2	4.725	Sn	3d3/2	3.15
O	1s	2.93			

Corrected area (Ix/Sx) = $\frac{Raw\ area}{Sensitivity\ factor}$.....(2)

Table S2: XPS fitting results and calculated values in RuSn SAO sample

Element	Position	FWHM	Raw area	Corrected area	Mean area	Splitting
Ru $3d_{3/2}$	284.43	1.28	1040.232	203.97	183.38	4.19
Ru $3d_{5/2}$	280.24	0.62	848.2077	114.78		
Ru 3p1/2	485.37	3.47	684.0043	178.59		
Ru3p3/2	462.82	4.11	1600.984	236.13		
Sn $3d_{3/2}$ (+4)	496.12	0.77	2700.353	857.25	722.50	9.04
Sn $3d_{3/2}$ (+2)	495.43	0.69	1964.053	623.51		
Sn $3d_{5/2}$ (+4)	487.78	0.66	2884.464	610.47		
Sn $3d_{5/2}$ (+2)	487.08	0.73	3774.213	798.78		
O 1s	531.8	2.16	1121.202	382.66	474.78	
	531.05	1.17	1661.987	567.23		

Table S3: Estimated elemental composition of RuSn SAO sample.

Element	Ru	Sn	O
Atomic %	13.3	52.32	34.38

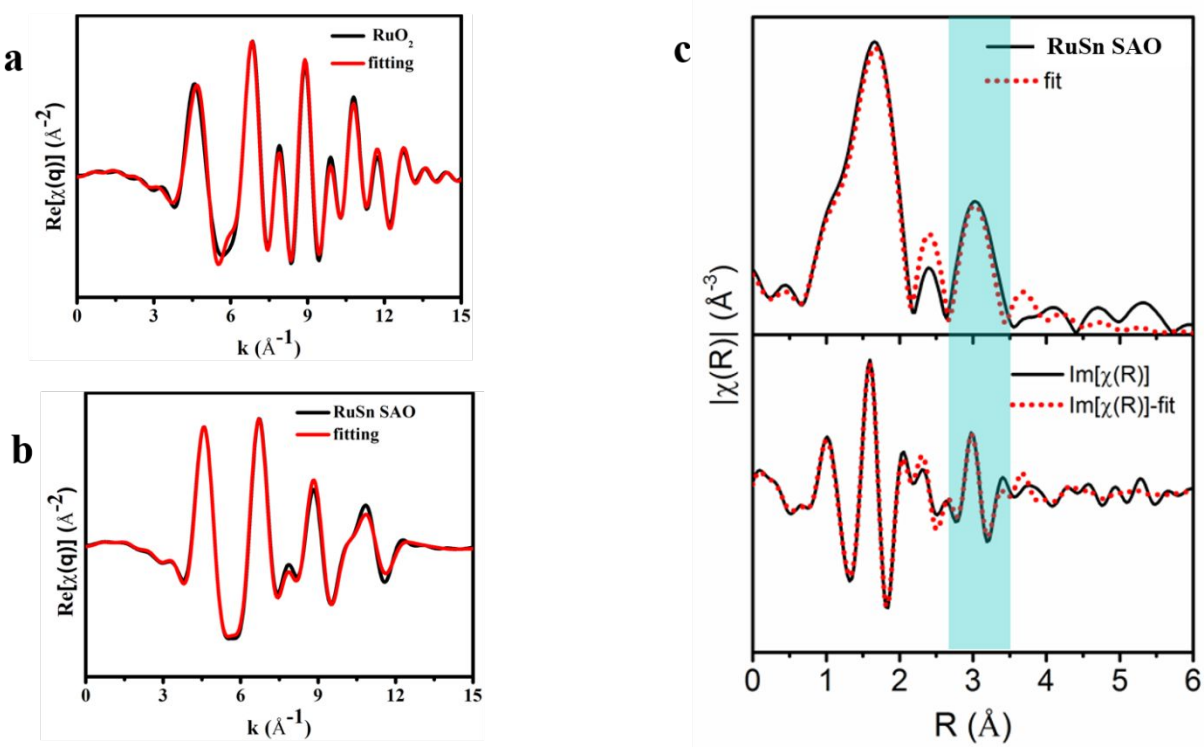

Figure S4. EXAFS fitting spectra. (a) K2-weighted EXAFS spectra of for RuO_2 (b) K2-weighted EXAFS spectra of RuSnSAO. (c) F.T-EXAFS spectra of RuSnSAO.

Table S4. FT-EXAFS analysis results for the RuO_2 and RuSn SAO.

Catalyst	Shell	N	R (Å)	ΔE_0 (eV)	σ^2 (Å^2)	R-factor ($\times 10^{-3}$)
RuO_2	Ru-O (1st shell)	6.0±0.8	1.98±0.01	-1.7	0.003	5.9
	Ru-Ru (1st shell	2.0±0.3	3.10±0.01	-13.4	0.003	
	Ru-Ru (2nd shell)	8.0±0.7	3.55±0.01	-4.8	0.002	
RuSn SAO	Ru-O	5.5±0.8	2.00±0.03	-0.4	0.004	6.1
	Ru-M	2.8±1.0	3.12±0.05	-12.0	0.007	

Note: N is the coordination number of each shell; R is the bond length; σ^2 is the Debye-Waller factor.

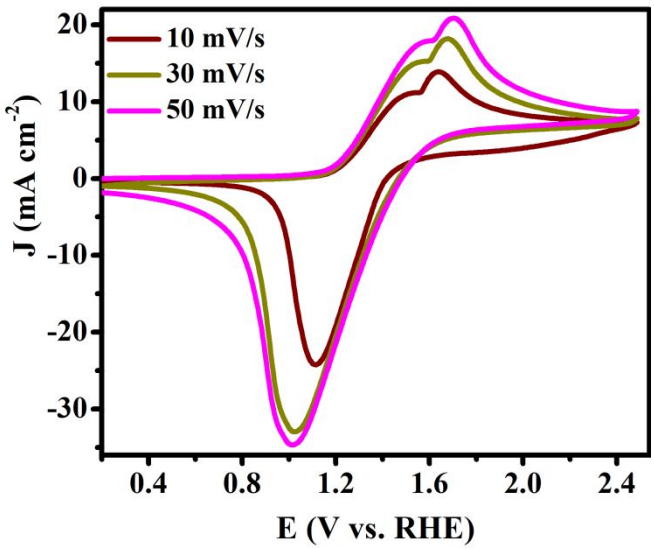

Figure S5. Cyclic voltammetry for commercial Pt/C in IOR at different scan rates.

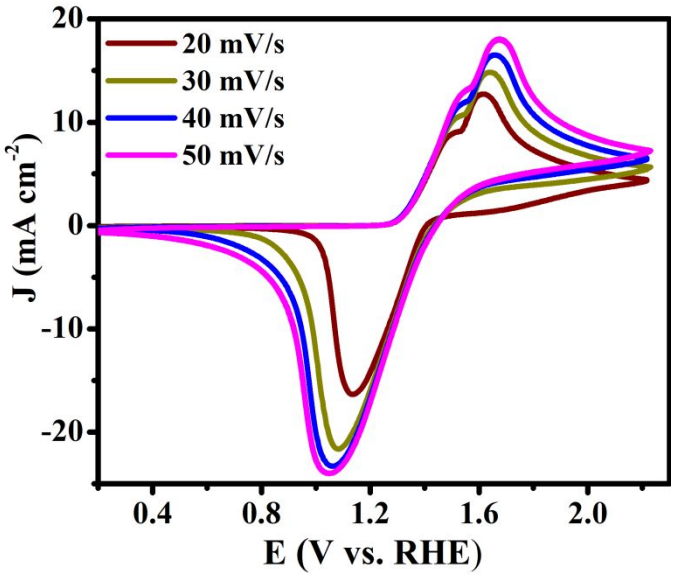

Figure S6. Cyclic voltammogram for SnO_2 in IOR at different scan rates.

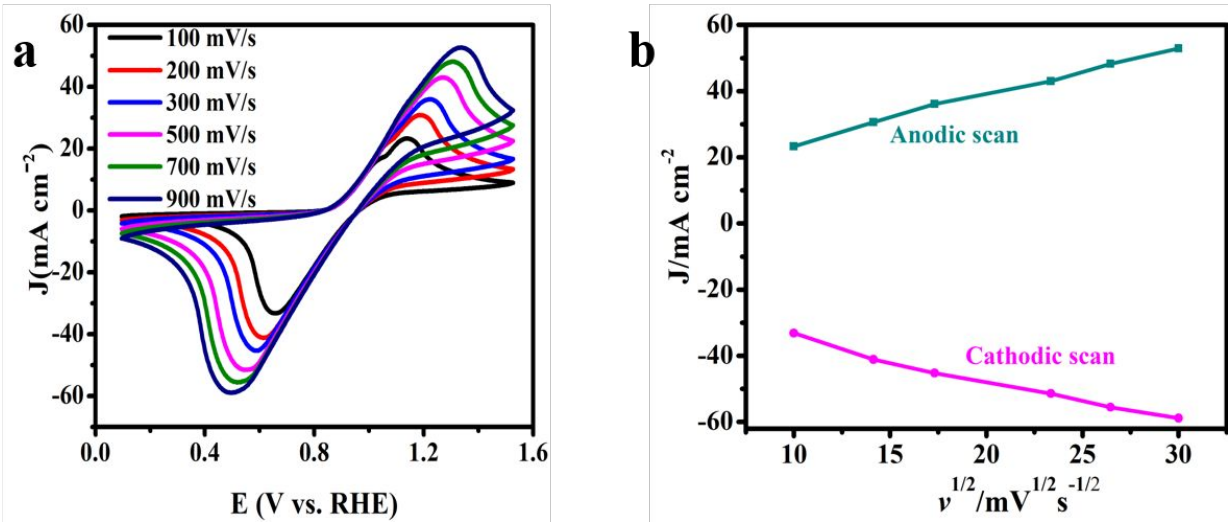

Figure S7. (a) CV for IOR at the different scan rates for the RuSn SAO electrocatalyst. b) Current density plotted against the scan rate.

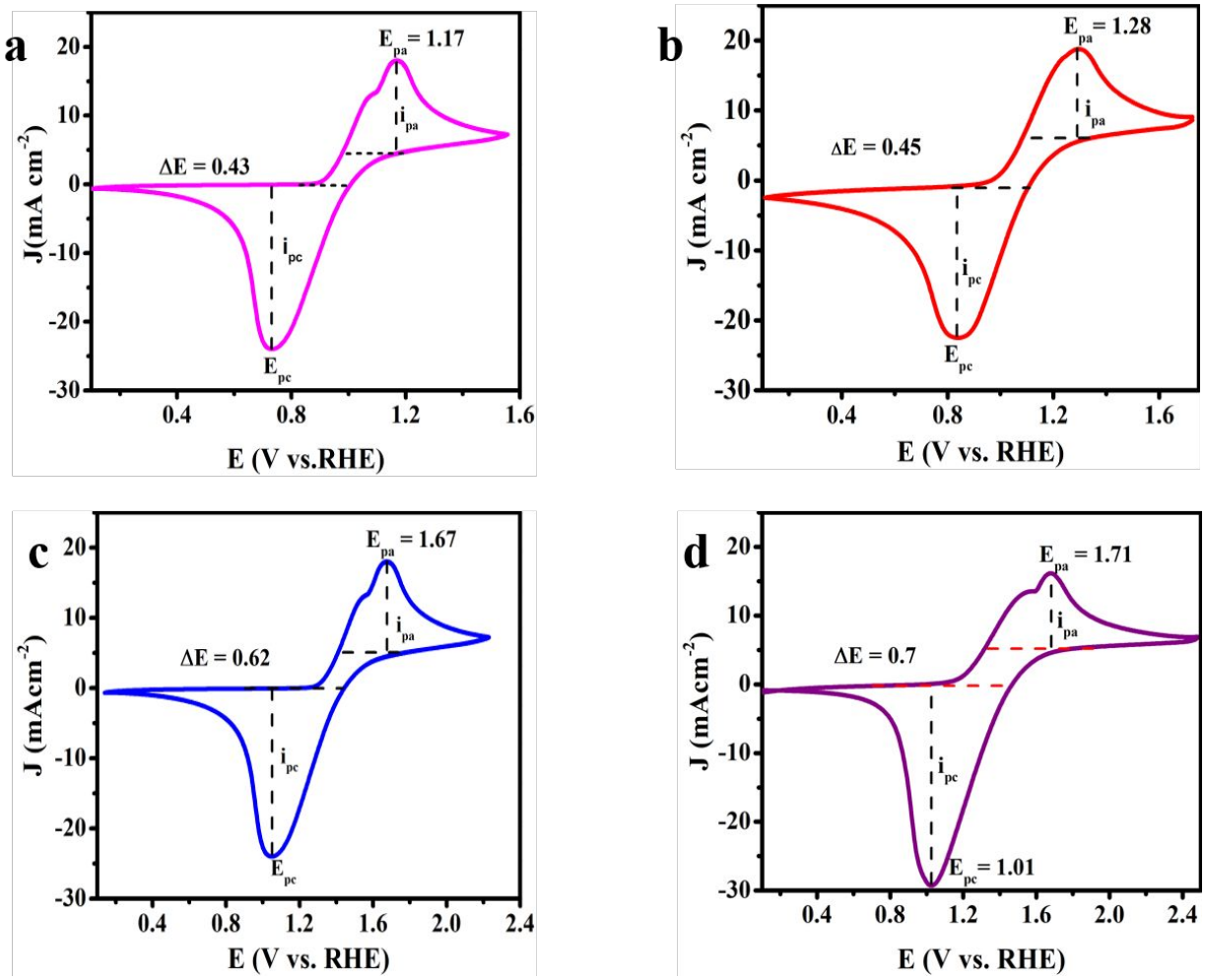

Figure S8. Peak-to-peak separation potentials at scan rate of 50 mV/s. (a) RuSn SAO (b) RuO_2 and (c) SnO_2 (d) Pt/C.

Table S5. Summary of electrochemical surface area, roughness factor, double layer capacitance and mass activity.

Catalyst	Cdl ($mF\ cm^{-2}$)	Roughness factor (Rf)	ECSA (cm^2mg^{-2} cat)	Mass activity ($mA\ mg^{-1}$ cat)
RuO_2	0.44	6.67	33.35	61.9
SnO_2	0.24	4.00	20.00	57.65
RuSn SAO	2.35	39.17	195.85	182.50

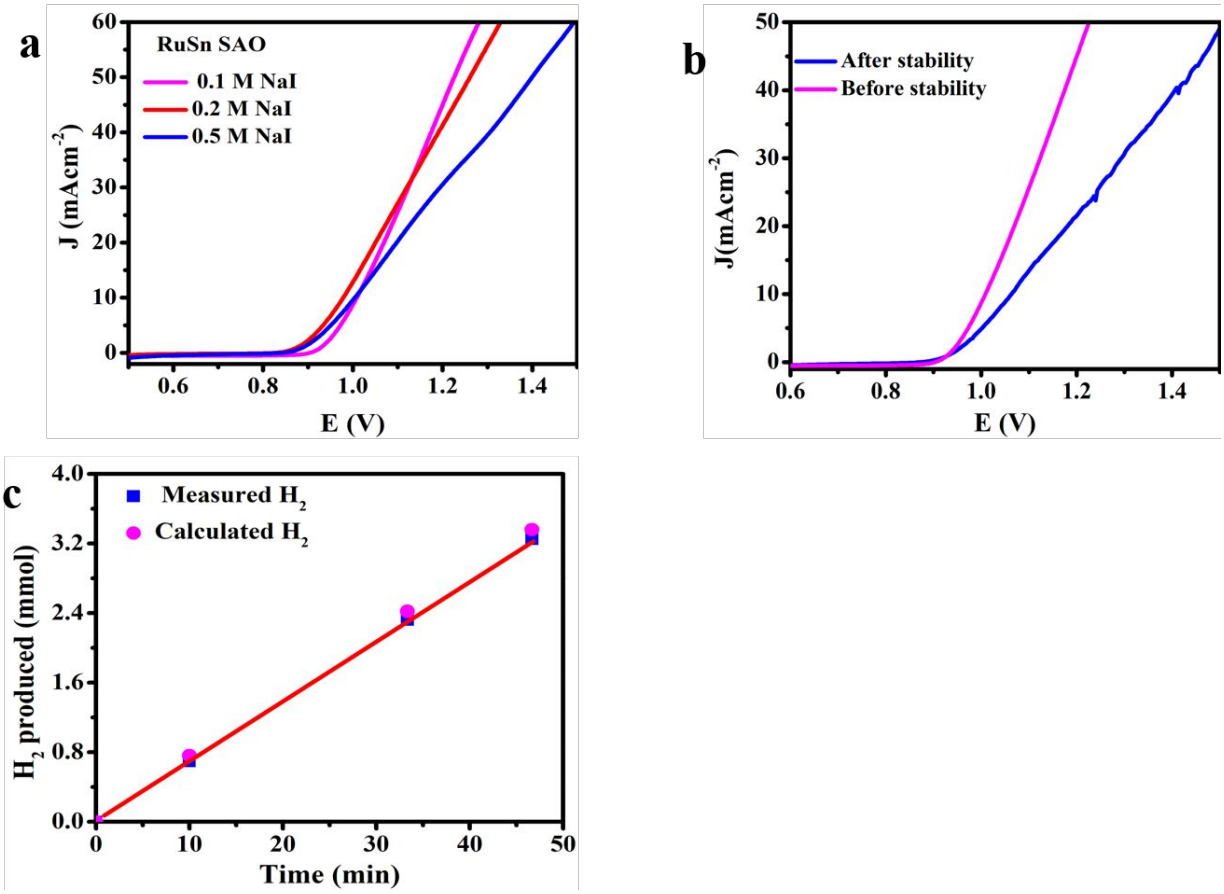

Figure S9. (a) LSV curves for RuSn SAO in 0.1 M $HClO_4$ with different NaI concentrations (b) (f) LSVcurves of RuSn SAO before and after stability in 0.1 M $HClO_4$ with NaI solution. (c) Rate of hydrogen production per time of electrolysis.

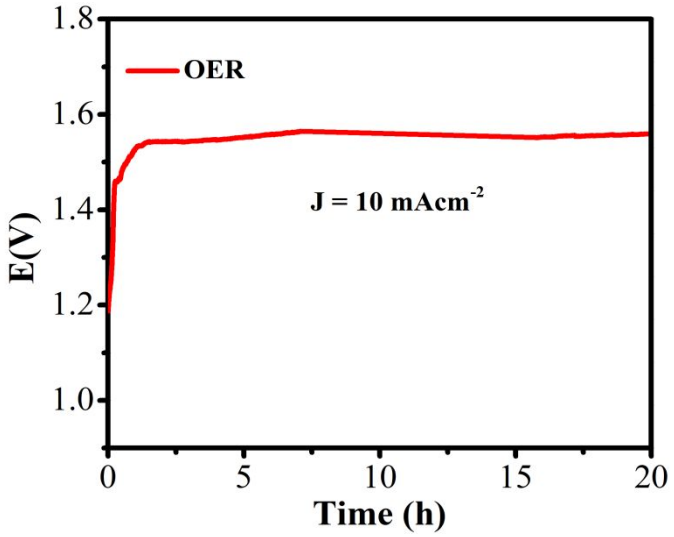

Figure S10. Chronopotentiometric stability for OER at applied current density of 10 $mAcm^{-2}$.

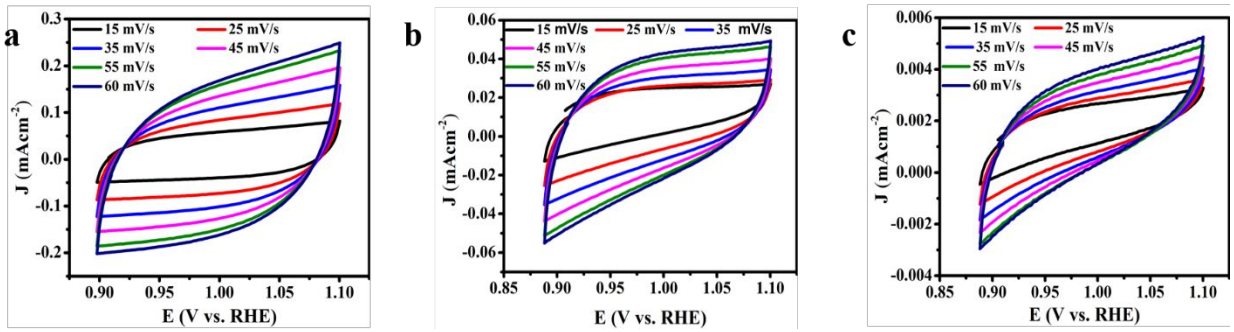

Figure S11. CV curves for these prepared samples on carbon paper. Non-Faradaic scan for double-layer capacitance with respective R^2 values. (a) RuSn SAO (b) RuO_2 (c) SnO_2

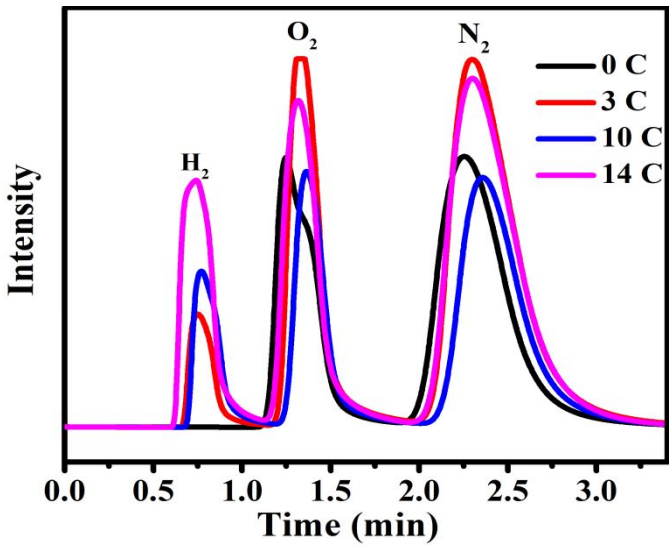

Figure S12. Hydrogen detection by gas chromatography (GC).

Table S6. Electrochemical performance of Ru-based oxide electrocatalysts for IOR-based electrolysis developed in this work and for OER-based electrolysis reported in literatures.

OER or IOR Catalysts	Electrolyte	Overpotential (mV)	Cell Voltage (at 10 $mAcm^{-2}$)	Tafel slope (mV dec^{-1})	Stability	Rf
$Cr_{0.6}Ru_{0.4}O_2$	0.5 M H_2SO_4	η_{10} = 178		56	10 h	OER[1]
Cu-doped RuO_2	0.5 M H_2SO_4	η_{10} = 188		43.96	8 h	OER[2]
$Ru_{0.5}Ir_{0.5}O_2$	0.1 M $HClO_4$	η_5 = 320				OER[3]
$Sr_{0.9}Na_{0.1}RuO_3$	0.1 M $HClO_4$		1.4 V	40	20 cycles	OER[4]
$W_{0.2}Er_{0.1}Ru_{0.7}O_{2-\delta}$	0.5 M H_2SO_4	η_{500} = 275		66.8	500 h	OER[5]
$Y_2Ru_2O_{7-\delta}$	0.1 M $HClO_4$		1.42 V	55	8 h	OER[6]
$CaCu_3Ru_4O_{12}$	0.5 M H_2SO_4			40	24 h	OER[7]
RuSn SAO	0.1 M $HClO_4$ + 0.1 M NaI	η10 = -220	1.07 V	45	20 h	**IOR This work**

Note: η10 = -220 mV is the difference between the standard potential for OER and the applied potential at 10 $mAcm^{-2}$ for IOR-based electrolysis.

Table S7. Summary of electrochemical parameters of catalysts in IOR obtained from CV and LSV curves.

Catalyst	E_{pa} (50 mV/s)	E_{pc} (50 mV/s)	ΔE_{IOR} (50 mV/s)	E_{onset} (v)	E_{IOR} (V) (at 10 $mAcm^{-2}$)	Tafel slope (mV dec^{-1})
RuSn SAO	1.17	0.74	0.43	0.92	1.01	45
RuO_2	1.28	0.83	0.45	1.01	1.26	67
SnO_2	1.67	1.05	0.62	1.20	1.32	83
Pt/C	1.71	1.01	0.7	1.19	1.30	70

Note: ΔE_{IOR} is peak to peak separation potential at scan rate of 50 mV/s; E_{onset} is the IOR onset potential; E_{10} is the IOR potential required to reach benchmark current density of 10 $mAcm^{-2}$.

Table S8. Metal analysis by ICP-MS from RuSn SAO sample.

Sample	Ru (ICP)	Sn (ICP)	Ru (Wt%)	Sn (Wt%)
RuSn SAO	0.366*5=1.83	5.320*5=26.6	6.4	93.6

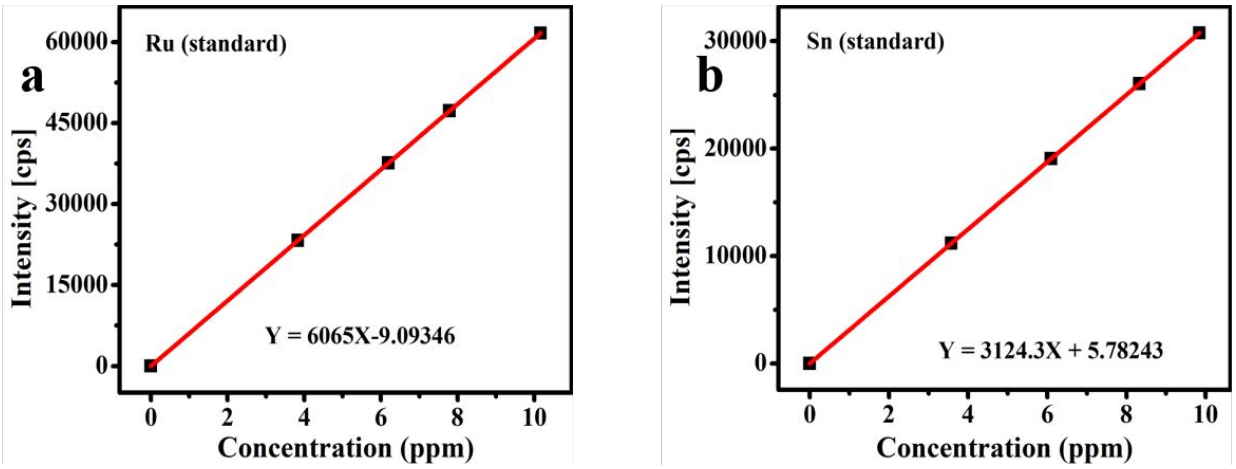

Figure S13. ICP-MS calibration curves for (a) Ru and (b) Sn elements.

References

(1) Lin, Y.; Tian, Z.; Zhang, L.; Ma, J.; Jiang, Z.; Deibert, B. J.; Ge, R.; Chen, L., Chromium-ruthenium oxide solid solution electrocatalyst for highly efficient oxygen evolution reaction in acidic media. *Nat.Comm.* **2019,** *10* (1), 1-13; https://doi.org/10.1038/s41467-018-08144-3.

(2) Su, J.; Ge, R.; Jiang, K.; Dong, Y.; Hao, F.; Tian, Z.; Chen, G.; Chen, L., Assembling Ultrasmall Copper-Doped Ruthenium Oxide Nanocrystals into Hollow Porous Polyhedra: Highly Robust Electrocatalysts for Oxygen Evolution in Acidic Media. *Adv. Mater.* **2018,** *30* (29), 1801351; https://doi.org/10.1002/adma.201801351.

(3) McCrory, C. C.; Jung, S.; Peters, J. C.; Jaramillo, T. F., Benchmarking heterogeneous electrocatalysts for the oxygen evolution reaction. *J. Am. Chem.Soc.* **2013,** *135* (45), 16977-16987; https://doi.org/10.1021/ja407115p.

(4) Retuerto, M.; Pascual, L.; Calle-Vallejo, F.; Ferrer, P.; Gianolio, D.; Pereira, A. G.; García, Á.; Torrero, J.; Fernández-Díaz, M. T.; Bencok, P., Na-doped ruthenium perovskite electrocatalysts with improved oxygen evolution activity and durability in acidic media. *Nat.Commun.* **2019,** *10* (1), 1-9; https://doi.org/10.1038/s41467-019-09791-w.

(5) Hao, S.; Liu, M.; Pan, J.; Liu, X.; Tan, X.; Xu, N.; He, Y.; Lei, L.; Zhang, X., Dopants fixation of Ruthenium for boosting acidic oxygen evolution stability and activity. *Nat.Commun.* **2020,** *11* (1), 1-11; https://doi.org/10.1038/s41467-020-19212-y.

(6) Kim, J.; Shih, P.-C.; Tsao, K.-C.; Pan, Y.-T.; Yin, X.; Sun, C.-J.; Yang, H., High-performance pyrochlore-type yttrium ruthenate electrocatalyst for oxygen evolution reaction in acidic media. *J. Am. Chem. Soc.* **2017,** *139* (34), 12076-12083; https://doi.org/10.1021/jacs.7b06808.

(7) Miao, X.; Zhang, L.; Wu, L.; Hu, Z.; Shi, L.; Zhou, S., Quadruple perovskite ruthenate as a highly efficient catalyst for acidic water oxidation. *Nat.Comm.* **2019,** *10* (1), 1-7; https://doi.org/10.1038/s41467-019-11789-3.